PSA-64 POWER SPECTRUM

Zaki S. Ali[1], Aaron R. Parsons[1,2], Adrian Liu[1], Jeff Zheng James E. Aguirre[3], David R. DeBoer[2], Daniel C. Jacobs[8], David F. Moore[3], Jonathan C. Pober[4],

Draft version August 3, 2014

ABSTRACT

Subject headings:

1. INTRODUCTION

The Donald C. Backer Precision Array for Probing the Epoch of Reionization (PAPER) is a dedicated experiment to measure the power spectrum of highly redshifted 21 cm emission during the Epoch of Reionization. PAPER is but one experiment that aims to detect this faint signal. Other telescopes that have the same goal are the Giant Meter-wave Radio Telescope (GMRT), the LOw Frequency ARray (LOFAR), and the Murchison Widefield Array (MWA). PAPER currently consists of 128 dual-polarization antennae in a 100-200MHz band out in the Karoo desert in South Africa.

The current best upper limit on 21 cm signal level is at $(41mK)^2$ which was measured by PAPER. This limit was acheived by using the delay-spectrum technique to remove foregrounds and by using a maximum redundancy array to essentially measure the same k-modes repeatedly, boosting sensitivity. In this analysis we employ the same techniques mentioned as well is introduce an optimal fringe-fringe rate filter to boost sensitivity and make use of precise calibration via the Omnical redundant calibrator package.

The paper is outlined as follows. In section **??** we describe the observations used in this analysis. In **??** we discuss the improvements in this pipeline with respect to the previous analysis of PSA-32 **?**. We then move on to the data analysis pipeline in section **??**. Seciton **??** describes the results of our efforts and provides new contraints on EoR. We conclude in **??**.

2. OBSERVATIONS

?? Here, we describe the features of the data set used in this analysis. Currently, PAPER boasts a modest 128 dual-polarization antenna array, which was followed by a 64 antenna array. This paper focuses on the latter. We used a maximally redundant configuration of the PAPER array (see Figure 1 for this analysis, relying on all of the redundant baselines for the calibration procedure, but only using a subset of the baselines for the power spectrum analysis. The columns are separated by 30 meters and the rows by 5 meters. For the power spectrum analysis we are using the baselines that correspond to the width between two columns (e.g. 49-41) as well as those that correspond to over and up and down one antenna (e.g. 10-41 and 10-58, respectively). These 154 baselines

are instantaneously redundant and therefore they measure the same Fourier modes on the sky. Within a single group of the three types of baselines above, the measurements add coherently, where between groups they add in quadrature. Having repeated measurements of the same baseline type greatly increases sensitivity.

The observation of this 64 antenna data set spanned a 135 day period that commenced on 2012 November 8 (JD62456240) and ended 2013 March 23 (JD62456375). Each baseline instantaneously measured the 100-200 MHz band which was divided into 1024 frequency channels of resolution 97.66 kHz and integrated for 10.7 seconds. In this analysis we analyze observations that spanned, in local siderial time (LST), a range of 1:00 to 10:00 hours. This range corresponds to the "EoR cold patch", in which galaxtic synchrotron power is minimal (away from the center of the galaxy).

3. SUMMARY OF IMPROVEMENTS FROM PSA32

In comparison to the previous PAPER pipeline (see **?**), this analysis took a slightly different approach which included some important steps to improve our bottom line. In short, the improvements included using a new, refined redundant calibration method (Zheng 2014), increasing the width of the wideband delay filter that removes smothe spectrum foregrounds, weighting the lst binned data sets, and optimal fringe rate filtering. In section **??**, we dicuss each of the improvements in more detail.

Figure **??** (TBD) shows the power spectra when each of the steps mentioned above are turned off and for the one where all of them are turned on. We can see the gradual improvement of the power spectra (hopefully).

4. ANALYSIS

Describe the overall flow of the data through of the pipeline. Here we describe the analysis pipeline of the data set obtained in 2012/2013 observing season. Data was first run through a preprocessing compression pipeline which reduces the volume of the data by a factor of forty. Afterwards we calibrate the relative phases of our array on the basis of redundancy using a logcal approach in delay space, and then get the absoultue phase calibration by fitting. We then set the flux scale of our observations by using Pictor A. The logcal done above was a rough estimate of the phase calibration and hence we used Omnical to get the calibrations to higher accuracy. This was a major difference in the pipeline from previous iterations on PAPER data. We then remove foregrounds using the delay filtering technique and form power spectra. The detalis of the above are discussed below and figure **??** shows a block diagram of the analysis

[1] Astronomy Dept., U. California, Berkeley, CA
[2] Radio Astronomy Lab., U. California, Berkeley, CA
[3] Dept. of Physics and Astronomy, U. Pennsylvania, Philadelphia, PA
[4] Physics Dept. U. Washington, Seattle, WA
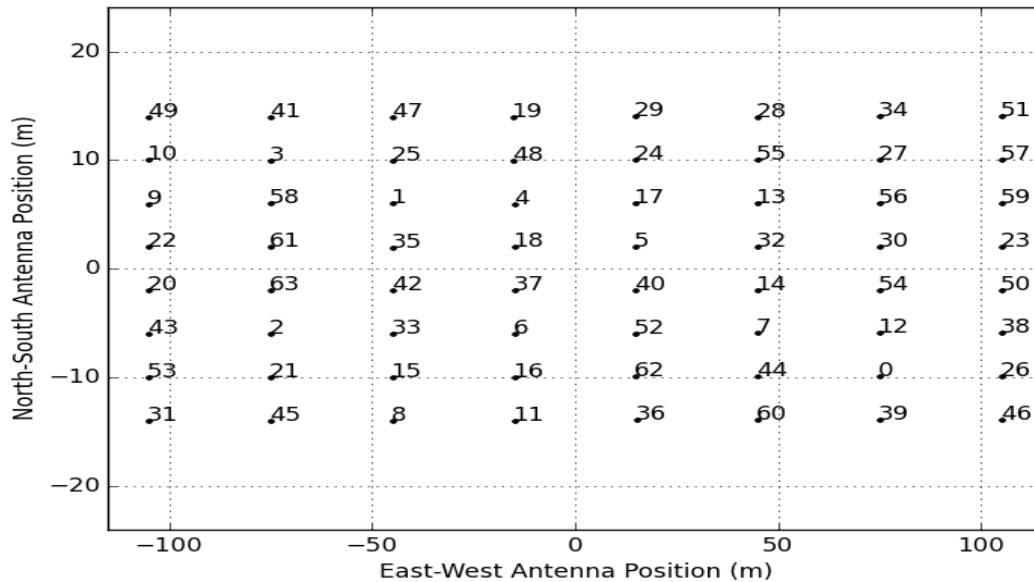[8] School of Earth and Space Exploration, Arizona State U., Tempe, AZ

Fig. 1.— Antenna positions for the PAPER 64 observation run.

pipeline.

4.1. *Preprocessing Compression*

As low frequency interferometer grow bigger, data volume becomes an issue. For this data set a 10 minute file consisting of 1024 channel complex visibilites integrated for 10.7 seconds each, requires 4G of storage space. For the observing season this requires about 40TB of storage space. This is doable, for now, but when it comes to analyzing sorting through this much data can be cumbersome. Therfore we have implementd a compression techinque which reduces the amount of storage by a factor of forty. Details of this critical step are presetned in the appendix A of (**?**). The punch line is that after RFI flagging, and removing unsmooth and transient emission from the data, we end up with a factor of 20 reduction in data volume, ending up with a total data set that requres 2TB of storage. After compression, it ends up that the orignal 1024 channels get downsampled to 203 channels (still encompassing the 100 MHz) and the 60 time samples per 10 minute file end up as 14 timesamples with an effective integration time of 42.8 seconds.

(Show plot of rraw data and compressed data?)

4.2. *Calibrations*

4.2.1. *Overview*

Precise calibration turned out to be critical in improving our bottom line of our final result. We began the calibration procedure by first using a logarithmic calibration scheme based in redundant measurements ((**?**), (**?**)) as well as using standard interferometric self calibration. We set the flux scale of the observations to Pictor A ((**?**) which has the spectrum

$$S_\nu = 382(\frac{\nu}{150MHz})^{-.76} Jy. \tag{1}$$

We then apply the solutions and run through another round of calibration. We use the methods described in

(**?**) and (**?**) to use a linearized redundant calibration. Specifically, we used a pre production version of the Omnical package described in (**?**).

4.3. *The logcal*

Before we begin the fine calibration, we perform the same calibration that was done in (**?**). That is, we use redundncy to do a relative phase[6] calibration between antennas, which removes the electrical delays from cables in the signal path. Due to redundancy, we cal calibrate out all of the per-antennas delays in the signal path relative to two parameters which we call τ_{ns} and τ_{es}. These delays are the relative electrical delays that correspond to baseline delays in the north-ssouth and east-west component for 2 reference baselines (49-10 and 49-41,respectively). The antenna based delay solutions vary as much as a couple nanoseconds day to day when solutions are averaged over hour long timescales withing a day. However, the variations in solutions is worse when only averaging over ten minute time scales. . Therefore need for better calibration is requred. We use self calibration to derive the two unknow parameters, τ_{ns} and τ_{ew}, by using Centaurus A, Fornax A, and Pictor A.

Note that there is no possibility of signal loss (see (**?**)).

4.4. *Gain Calibration*

Gain calibration was derived on the basis of redundancy and self calibration. The phase calibrations described above, simultaneously also calibrated for the gain variation between antennas. Again we can only calibrate to a fiducial antenna (49) whose gain is defined as unity. We then perform a self calibration to set the flux scale to Pictor A whose spectrum is derived in (**?**). We use the same methods describes in (**?**).

Figure **??** shows that dataset beamformed to Pictor A, with log janskies on the y axis and lst on the xaxis for

---

[6] In actuality, we solve for delays to get around phase wrapping issues. These delays are applied to visibilities as $e^{2\pi i \tau \nu}$

a frequncy of .1 + (120/203)*.1/203. As can be seen, the day to day variation in the formed beam has a fractional spread of about 10%. This shows the stability of the instrument and the well behaved calibration solutions derived above.

4.5. *Omnical*

(How did we know that our calibrations was not good enough? Because of the power spectrum? PSA32? We did beamform data to pictorA and say that vs LST, the beamform matched well day to day with a fractional spread of about 10The 10% spread in the formed beam to Pictor A in figure **??** shows the stability of the solutions over time. However, we wanted to do better. The new element to our calibration pipeline was the use of the omnical package developed at MIT by Jeff Zheng ((**?**)). This calibration pipeline takes redundant calibration one step deeper by performing lin cal, which solves for the unbiased phase and gain solutions.

Omnical performs a logcal first to find biased phase and gain solutions so the solutions are close. lincal, in order to converge, requres a guess of the solutions that are close to the actual value. Logcal delivers this result. Because of the calibration performed above, which was an implementation of logcal, the data requried for lincal was already in hand. Lincal was ran on the data and the solutions were applied to the data.

Figure **??** shows the gain solutions output by omnical.

4.6. *lstbinning*

The Omnical calibration pipeline removes all of the variation between unique baseline types and averages them together, effectively creating a model for what a baseline measures. This is not simulated and is derived from the data. These averaged models are what we use to continue through the analysis pipeline.

The motivation for using these datasets is that they are pre calibrated and have baseline to baseline variation removed from them, including cross talk and other systematics. This is essentially the averaged of what a unique baseline type should measure. This includes RFI events that effect the entire array and sky signal.

We lstbin these data into lst bins of 42.8 seconds over the entire observation.

4.7. *WB delay filtering*

Galactic synchrotron and extragalactic point sources, generally foregrounds, greatly contaminate the EOR signal. They are roughly 9 orders of magnitude (Pober 2013a) above the expected level of EOR and can hide low order RFI events and cross-talk. Therefore, its removal is completeley necessary and required in order to obtain the desired EOR signal. In addition to dominating the EOR signal, foregrounds can corrupt higher-order k modes in the power spectrum measurement from the sidelobes arising from RFI flagging and the finite bandwidth used in the line of sight Fourier transform (corresponding to $k_{\parallel}$).

PAPER uses the delay filtering technique described in (**?**) to remove smooth spectrum foregrounds that mask EOR. This method relies on the fact that for a given baseline, there is a maximum delay a source can be measured at. This maximum delay is given when the source is on the horizon. Since the delay is given by projection of the baseline in the direction of the source, the maximum delay is just the time it takes light to travel the baseline length. Following the technique described in (**?**), the delay transform of a visibility takes the form

$$\tilde{V} = \int W(\nu)S(\nu)V(\nu)e^{-2\pi i\tau\nu}d\nu, \qquad (2)$$

where $V(\nu)$ is the visibility measured, $W(\nu)$ is a blackman-harris windowing function and $S(\nu)$ is the weighting function that encodes the flags for the data. Hence, the the fourier transoform of the source spectrum convolves the foruier transform of the visibility. Therfore, this method localizes smooth spectrum sources which have a narrow footprint in delay domain. Luckily, most extragalactic sources and synchrotron radiation have power law spectra.

Using the entire bandwidth increases the degree of foreground separation and is impereative to get the best estimate of foreground isolation. We apply the delay transform defined above to every baseline over the entire 100 Mhz. Figure **??** shows the localization of foregrounds for a 30 meter baseline within the horizon of 100 ns. After the filter is applied we see 3 orders of magintude in reduction of foreground isolation. This is a factor of 6 in powerspectra!

Following the method in (Parsons Backer 2009), we use a CLEAN algorithm to deconvolve out the effects of RFI flags and band edge effects. FRI flags and the band edges have the effect of scattering foreground emission to higher order delay modes which would otherwise be uncontaminated. The implementation of CLEAN is such that it treats the RFI flags as a sampling function in frequency and iteratively fits to the highest point in delay space, and therefore trying to fill in the flagged data in frequency. We restrict these CLEAN components to fall within 100 ns of the horizon limit for a given baseline. This CLEAN model is then subtracted off from the the orignal visibility, leaving us with a filterd visibility.

4.8. *optimal Fringe-rate filter*

Before forming power spectra we need to time average visibilities that measure the same k mode on the sky. This is the best way to combine data because we get a $\sqrt{N}$, where N is the number of samples, gain in sensitivity. This is in oppostion to weighting after forming power spectra, where noise beats down as the $\sqrt{N}$. Rather than a straight averaging in time, we can do better by using a weighted averge. Specifically, we want to upweight samples that have higher signal-to-noise.

This is acheived by applying a carefully crafted filter in fringe rate domain, the fourier dual to time. Different patches on the sky correspond to different fringe rates, for a given baseline and frequency. Maximum fringe rates are found along the equatorial plane where zero fringe rates are found around the poles (sources at the poles do not move through the fringes of a baselines). Sources on the other side of the pole, corresponds to negative fringe rates, because they move through the fringe pattern in the opposite direction. By weighing the fringe rates sampled by a baseline by the beam response of the baseline, gives us the optimal fringe rate filer to use for time averaging. See Parsons/Liu 2014 for a detailed discussion.
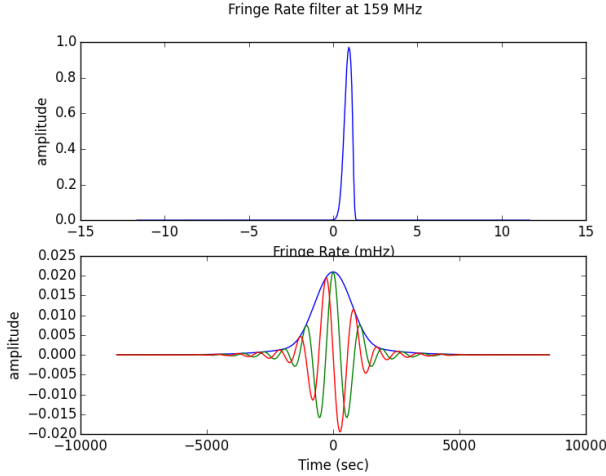
FIG. 2.— slice of a fringe rate filter at a frequency of 159MHz. Top is the filter in fringe rate domain. The bottom consists of the corresponding time domain filter gotten by fourier transforming and windowing with a blackman-harris window to damp the tails. **??**

We implement the optimal fringe rate filter by first calculating the fringe rate of everypoint on the sky and weighting it the beam of a given baseline, summing along constant fringe rate contours, This is then squared to get the effective sensitivity of each fring rate bin (squaringe the power beam). That is we are upweighting fringe rate bins that have greater signal-to-noise. We then fit a gaussian to the optimal filter to have a smooth function, along with tanh function for to have a smooth cut off at the maximum fringe rate for the given baseline and

frequency. Note that this only calculated for a given frequency and scaled to other frequencies, due to the fact that fringe rate scales linearly with frequency via

$$f_{max} = \frac{|\mathbf{b}_{eq}|}{c}\omega_\oplus\nu \qquad (3)$$

To minimize edge effects in time we fourier transform the optimal fringe rate filter to get the time domain convolution kernel and apply it to each visibility for a given channel and baseline.

The exact implementation of the optimal fringe rate filter, uses a convolution kernel of 400 integrations (should we be??). This has the effect of denoising the data as if it averaged over 4.75 hours with a weigthing function that is the beam weighted fringe rate. For each of the baseline types used (30 m baselines of different orientations).

Since the PAPER beam is 45 degrees, and the array is located at a declination of $-30°$ the fringe rates associated with the low signal to noise (down in the beam) correspond to very high and very low/negative fringe rates. Figure **??** shows a cut of the optimal fringe rate at MHz for a 30 m east west baseline. Therfore, the implemented fringe rate filter removes some sky signal, signal associated with fringe rates outside of the ranges shown in Figure **??**. Figure **??** shows that the applied filter removes sky associated with negative fringe rates and very high fringe rates.
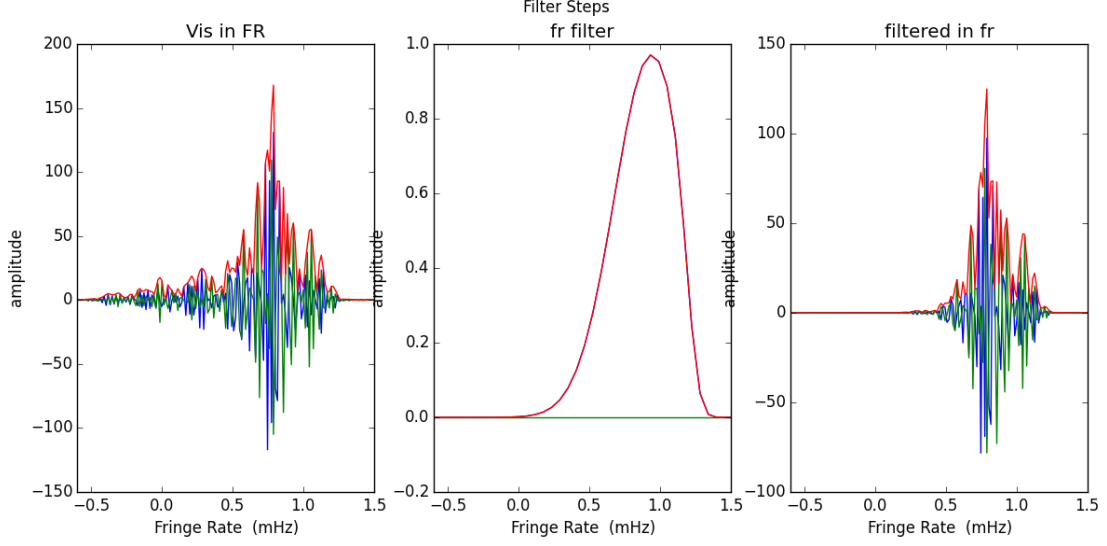
5. RESULTS

6. SCIENCE

7. CONCLUSIONS

Fig. 3.— slice of a fringe rate filter at a frequency of 159MHz. Shown here is the fringe-rate transform of foreground contained data for a 30 m east-west baseline. Blue and green are the real and imaginary part, respectively and red is the absolute valeu. Note the maximum and minimum fringerates correspond to the theoretical minimum and maximum for a baseline of this length at 159 MHz. The center panel shows the real (red) and imaginary (green) parts of the fringe rate filter to be applied. Finally, the last panel on the right shows that the fringe rate filtered visibilities. The fringe rate filter is just a weighting applied in fringe rate space and retains foregrounds.
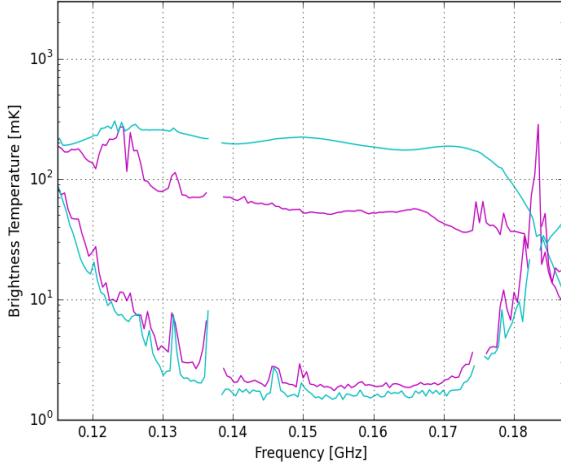
??

Fig. 4.— Estimates of noise temperature. Magenta is frequncy differenced estimate where the cyan is the time differenced estimate. All curves are averaged over all 30m east-west baselines (56) and averaged incoherently in 43s bins of LST from LST 2 to 5 hours with a channel bandwidth of 490 kHz.

??